Check for updates

Passive Jet Flow Control Method for Suppressing Unsteady Vortex Shedding from a Circular Cylinder

Wen-Li Chen, Ph.D.[1]; Xiangjun Wang[2]; Feng Xu, Ph.D.[3]; Hui Li, Ph.D.[4]; and Hui Hu, Ph.D.[5]

Abstract: A numerical simulation is performed to investigate a passive jet flow control method for suppressing the alternating vortex shedding from the circular cylinder. A hollow pipe is tightly set on the circular cylinder, and two arrangement cases for the holes are employed: one is a five-hole case, which means that five suction holes are set near the front stagnation point and five jet holes set near the rear stagnation point of the cylinder. The other is the full-hole case, which means the holes are equidistantly arranged on the hollow pipe. The incoming flow enters the suction holes and jets into the near wake from the outlet holes. Consequently, the wake vortex shedding alternately is manipulated or destroyed. The numerical simulations of baseline cases (without control) are first conducted to verify the reliability of the numerical model. Next, the two controlled cases (five hole-case and full-hole case) are investigated at the Reynolds number $R = 10^3 - 10^5$. It is found that a remarkable mitigation for the aerodynamic forces of the cylinder is revealed at the high Reynolds number: the in-line drag coefficient can be reduced by approximately 40.00%. At the same time, the cross-flow lift fluctuation has been completely suppressed with a control effectiveness of more than 98.00%. The swirling strength distributions and corresponding streamline results around the circular cylinder are then described, which are employed to present the essential physics regarding why the unsteady vortex shedding is suppressed by the passive control method. Finally, the stability of the flow field is discussed based on the linear stability theory. The absolute instability region near the cylinder shrinks substantially at the high Reynolds number, even changing into a convective instability region completely for the five-hole cases. **DOI: 10.1061/(ASCE)AS.1943-5525.0000661.** © *2016 American Society of Civil Engineers.*

Author keywords: Passive flow control; Aerodynamic force; Numerical calculation; Vortex shedding; Flow stability.

Downloaded from ascelibrary.org by Iowa State University on 09/23/22. Copyright ASCE. For personal use only; all rights reserved.

Introduction

In the past several decades, flow around a bluff body (i.e., a circular cylinder) has been an extensively researched topic. The aerodynamic characteristics for stationary circular cylinders were investigated based on a large number of numerical and experimental studies. The mean drag coefficient, Cd_{mean}, of the circular cylinder versus Reynolds number was studied by Wieselsberger (1921), Roshko (1961), and Munson et al. (2002). Bearman (1969) investigated the Strouhal number, S, against the Reynolds number (R) from $R = 1.0 \times 10^4$ to 1.0×10^7, based on the results shown by Relf and Simmons (1924), Delany and Sorensen (1953), Ribner and Etkin (1958), and Roshko (1961). Norberg (1994) studied the Strouhal number for a single circular cylinder through the experiments at $R = 1.0 \times 10^2$ to 3.0×10^5. Many investigations (Drescher 1956; Morkovin 1964; Blevins 1990; Ribeiro 1992) have also been conducted for lift fluctuations. A compilation on the root-mean-square lift fluctuations, Cl_{rms}, versus Reynolds number, R, was given by Norberg (2003).

Wake vortex shedding is well-known to alternately have an extremely key role in vortex-induced vibration (VIV). If alternating vortex shedding is suppressed, VIV will be prevented. Shih et al. (1993) modified the surface roughness of the circular cylinder at $R = 8 \times 10^6$. Bearman and Harvey (1993) measured the aerodynamic force and Strouhal number for a dimpled circular cylinder in the Reynolds number range of $R = 2 \times 10^4$ to 3×10^5. Lee and Kim (1997) studied the flow characteristics of a circular cylinder wrapping three small helical rubber wires. Anderson and Szewczyk (1997) mounted a splitter plate on the circular cylinder, which prevented the transverse moving of the wake near the cylinder. Lim and Lee (2002) conducted an investigation on the flow of a circular cylinder with longitudinal-grooved surfaces, i.e., U-shaped and V-shaped surfaces. Favier et al. (2009) used a self-adaptive hairy coating to cover the circular cylinder. It was observed that the drag force decreased by 15% roughly, and the lift fluctuation reduced around 40%. All of these mentioned control methods induce their effects by changing the surface of the object, which does not require additional power input. Thus, these approaches are passive control methods. Alternately, many control methods need a constant energy supplement. These methods can create different reactions for different situations because of mounted sensors and actuators, and they are thus called active control methods. Arcas and Redekopp (2004) numerically simulated the relationship between the jet/suction and the flow structures for a plane forebody by using a rectangular base. Chen et al. (2013, 2014) employed an active suction flow control method to manipulate the alternating vortex shedding from a cylinder and the corresponding VIV. Feng et al. (2010, 2011) and Feng and Wang (2010, 2012) pointed out that the synthetic jet could delay the flow separation and reduce the drag acting on bluff bodies.

[1]Professor, School of Civil Engineering, Harbin Institute of Technology, Harbin, Heilongjiang 150090, China (corresponding author). E-mail: cwl_80@hit.edu.cn

[2]Graduate Student, School of Civil Engineering, Harbin Institute of Technology, Harbin, Heilongjiang 150090, China. E-mail: wangxiangjun7437@163.com

[3]Assistant Professor, School of Civil and Environment Engineering, Harbin Institute of Technology, Shenzhen Graduate School, Shenzhen 518055, China. E-mail: xufeng_hit@163.com

[4]Professor, School of Civil Engineering, Harbin Institute of Technology, Harbin, Heilongjiang 150090, China. E-mail: lihui@hit.edu.cn

[5]Professor, Dept. of Aerospace Engineering, Iowa State Univ., Ames, IA 50011. E-mail: huhui@iastate.edu

Note. This manuscript was submitted on December 10, 2015; approved on May 2, 2016; published online on July 15, 2016. Discussion period open until December 15, 2016; separate discussions must be submitted for individual papers. This paper is part of the ***Journal of Aerospace Engineering***, © ASCE, ISSN 0893-1321.

The current passive suction/jet flow method does not requires active energy input and complicated equipment, which is superior to the active suction or blow control methods. The oncoming flow which passes through the hollow pipe blows into the wake from the jet holes. Consequently, the blowing air from the jet holes prevents the fluid behind the cylinder from undertaking transverse motion just like a partition wall, and the alternating wake vortex shedding is manipulated or broken. Therefore, the fluctuating lift can be eliminated or reduced and the potential vortex-induced vibration will be controlled. On the other hand, the jetting air flow injects energy into the wake, resulting in a reduction of the wake negative pressure, which leads to a lower drag force.

Computational Fluid Dynamics Numerical Models

Chen et al. (2016) employed numerical model to simulate the baseline case (without control), five-hole case, and full-hole case as shown in Fig. 1(a). The baseline case is to simulate the flow around a cylinder with a diameter of 100 mm. The passive control methods include the five-hole case and full-hole case. The arrangement of the five-hole case is such that five holes are located symmetrically near the front and rear stagnation points of the cylinder, separately. The width is set as 7.5° for each hole, which is the half of the central distance of the neighboring holes. The full-hole case is that 24 holes with the same width of 7.5° are equidistantly set on the pipe surface.

The Reynolds number varies from $\mathrm{R} = 1.0 \times 10^3$ to 2.0×10^5 in the present investigation. Reynolds-averaged Navier-Stokes (RANS) methods including the shear-stress transport (SST) k-ω and the transition SST turbulent models were employed to simulate the incompressible flow through the commercial software *ANSYS FLUENT 14.5*. The SST k-ω model which is employed for $\mathrm{R} = 1.0 \times 10^3$, $\mathrm{R} = 1.0 \times 10^4$, and $\mathrm{R} = 1.0 \times 10^5$ possesses the unique advantages to simulate the flow separation phenomenon (*ANSYS 14.5*). The transition SST model is a four-equation model with two SST k-ω transport equations, one intermittency equation, and one transition onset criteria transport equation. As a result, the transition SST model has a better result for simulation of the transition flow than the SST k-ω model does (*ANSYS 14.5*).

The pressure-based solver which is used for the incompressible flow is applied. The semi-implicit method for pressure linked equations consistent (SIMPLEC) algorithm, proposed by Vandoormal and Raithby (1984), is selected to solve the discrete equations. The second-order upwind is employed for spatial discretization. The second-order implicit algorithm is adopted for transient formulation.

Mesh of Computational Domain

The grid partitions of the flow field and the passive jet flow control pipe are shown in Fig. 1(a). The suction/jet flow control pipe wraps on the circular cylinder with the holes on the pipe surface (divided into the five-hole and full-hole cases). The incoming flow entering into the inlet holes and jetting into the near wake from the outlet holes will suppress or destroy the alternating wake vortex shedding.

The computational domain has been revealed by Chen et al. (2016). The distances between the inlet and outlet boundaries to the center of the cylinder are set as $10 \times \mathrm{D}$ and $30 \times \mathrm{D}$, respectively. The blocking ratio is accounted for 5.0% according to the computational domain with a transverse width of $20 \times \mathrm{D}$. The grid near the circular cylinder has been fined and smoothed. The perimeter of the cylinder is divided into 480 uniform cells, the first grid height near the cylinder is determined by $y^+ \approx 1$. The spanwise direction length is $0.5 \times \mathrm{D}$ which is uniformly distributed into 20 grids. The total grid number of the computational region is roughly 2 million, as shown in Fig. 1(b). The quality inspection of the grids is above 0.95 for the $3 \times 3 \times 3$ determinant and the minimum angle of the grids is approximately 45°.

The entrance is termed the velocity inlet. The pressure outlet is used for the export. Two sides are set into the moving wall. Up and down adopt the symmetry. The holes and pipe are set into the

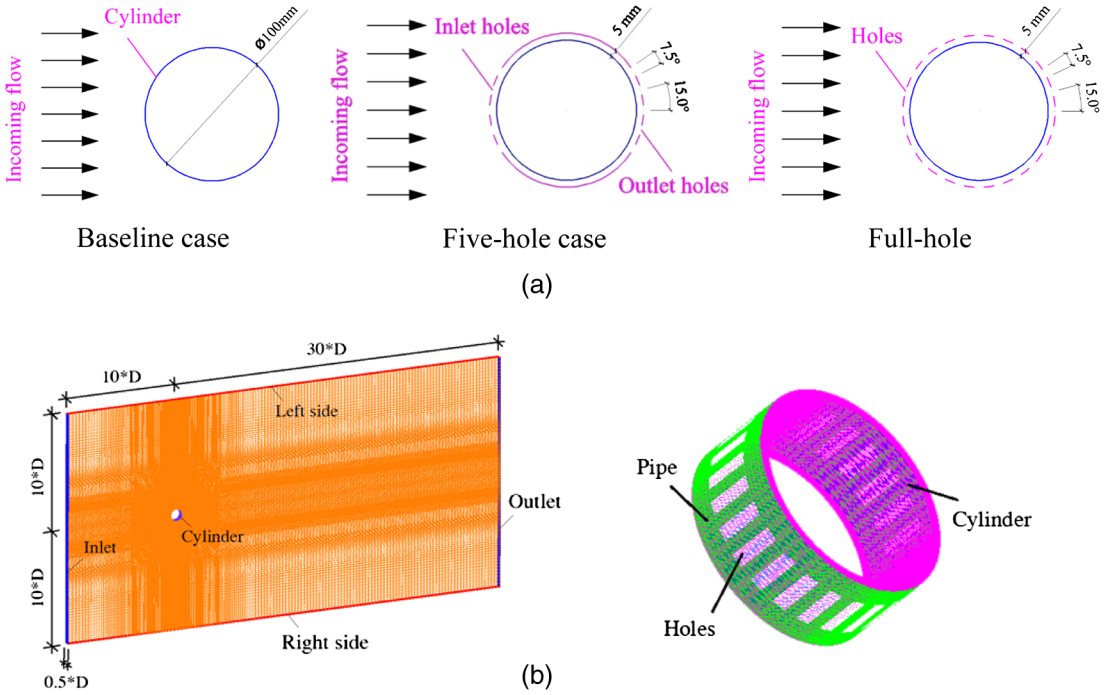

Fig. 1. Information on the numerical model of the passive jet flow control method (reprinted from Chen et al. 2016, with permission of Springer): (a) numerical models; (b) grid partitions of the flow field and passive jet flow control pipe (full-hole case)

J. Aerosp. Eng., 2017, 30(1): 04016063

Downloaded from ascelibrary.org by Iowa State University on 09/23/22. Copyright ASCE. For personal use only; all rights reserved.

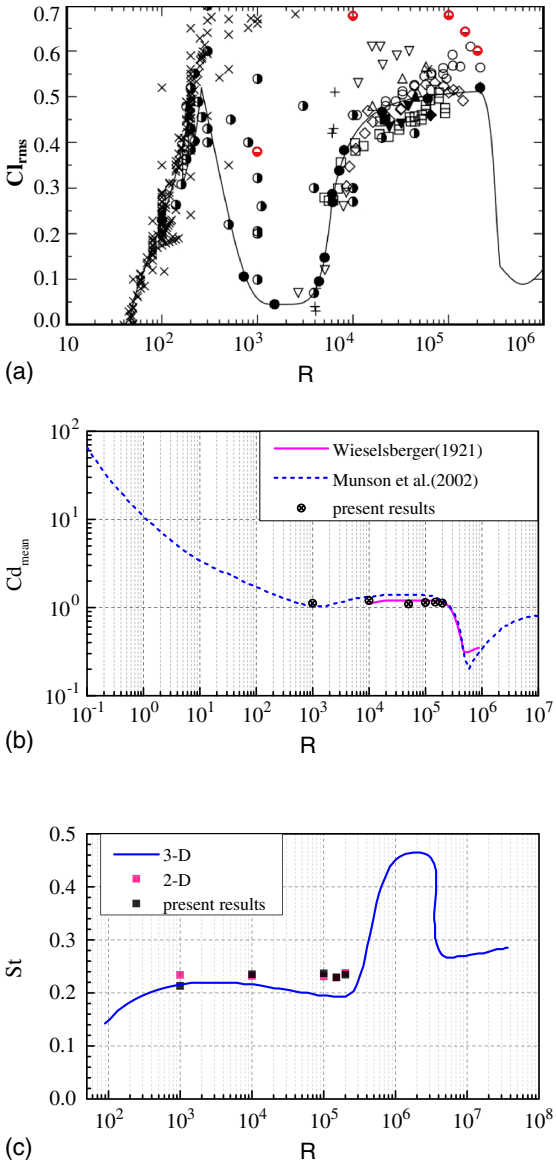

Fig. 2. Comparison of aerodynamic coefficients and the Strouhal number with previous results: (a) Cl_{rms} versus R [note: white square: Keefe (1962); plus: Leehey and Hanson (1971); black up-pointing triangle: Sonneville (1973); white up-pointing triangle: Mohr (1981); white down-pointing triangle: Moeller and Leehey (1984); black square: Gartshore (1984); white diamond: Szepessy and Bearman (1992); white circle: West and Apelt (1993); black diamond: Sakamoto and Haniu (1994); times: 2-D; circle with right half black: 3-D; black circle: Norberg (2003); solid line: empirical functions; circle with lower half black: present results]; (b) Cd_{mean} versus R; (c) S versus R

interior boundary, which the fluid can pass through in the baseline case. However, all holes are set into the interior boundary only for the full-hole case. Five holes are separately set into the interior boundary on the front stagnation point side and the rear stagnation point side for the five-hole case.

Numerical Model Validation

The baseline case is firstly carried out in order to validate the numerical model. The comparisons with the previous results of aerodynamic coefficients, the Strouhal number, S, and the flow separation points are first performed. The root-mean-square lift fluctuation, Cl_{rms}, against the Reynolds number is shown in Fig. 2(a).

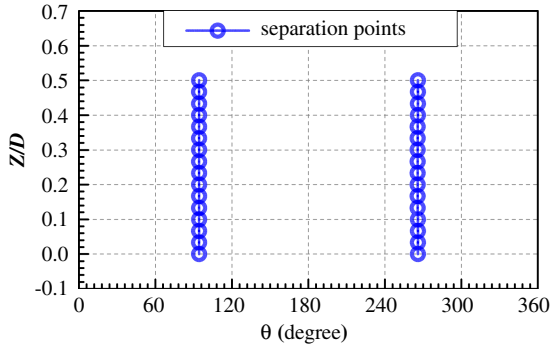

Fig. 3. Flow separation points ($R = 1.0 \times 10^5$)

The present Cl_{rms} is a little larger than the previous results due to a small length of the spanwise direction compared with the other two directions of the computational domain, which limits the development of three-dimensional (3D) flow. This phenomenon is more obvious as the Reynolds numbers become higher. Compared with the 3D flow, the two-dimensional (2D) flow has a better correlation in the spanwise direction. So, the 2D flows have larger Cl_{rms} with a high Reynolds number. Fig. 2(b) shows the mean drag coefficient, Cd_{mean}, is coincident with the previous results. For the Strouhal number, S, the previous experimental results of 3D flows are less than the present numerical simulation result at a high Reynolds number. However, it is taken into consideration that the height of the computational domain is very small. The 3D flow in the spanwise direction cannot develop fully. Therefore, it can be regarded as a 2D flow. Thus, Fig. 2(c) indicates the present S results are more consistent with the results of the 2D flow (Labbe and Wilson 2007; Al-Jamal and Dalton 2004). Fig. 3 shows the flow separation point results at $R = 1.0 \times 10^5$. The separation angle is approximately 94.25°, which is notably close to the results of Breuer (2000) (91.45–95.00°). Breuer (2000) performed a large eddy simulation (LES) to investigate the flow around a circular cylinder at $R = 1.4 \times 10^5$, where the mean drag coefficient and separation angle are both given, which are similar to the present results. From the preceding comparison, the present grids and numerical model are reliable and can be employed for further investigation of passive jet flow control.

Results and Discussion

Five-Hole Case

The numerical calculation of the five-hole case was then conducted. Fig. 4 shows the average pressure coefficient distributions on the midspan plane of the circular cylinder. In comparison with the baseline results, the distributions of the mean pressure coefficients on the circular cylinder have a great change, particularly for the absolute values of the negative pressure coefficients from the flow separation region to the rear stagnation point. The average pressure coefficients are greatly decreased when $R \geq 1.0 \times 10^4$. The drag reduction is then realized because the pressure drop between the front and rear stagnation points of the circular cylinder has been greatly decreased for the five-hole case.

The root-mean square (RMS) value of the pressure history is often employed to describe the pressure fluctuation which is related to the dynamic characteristics of lift forces acting on the circular cylinder. Fig. 5 shows the comparison of the pressure coefficient RMS results of the circular cylinder between the five-hole case and baseline result. It is found that the pressure coefficient RMS values reduce with increments of the Reynolds number for the five-hole case. For the baseline case, there are quite high pressure

Downloaded from ascelibrary.org by Iowa State University on 09/23/22. Copyright ASCE. For personal use only; all rights reserved.

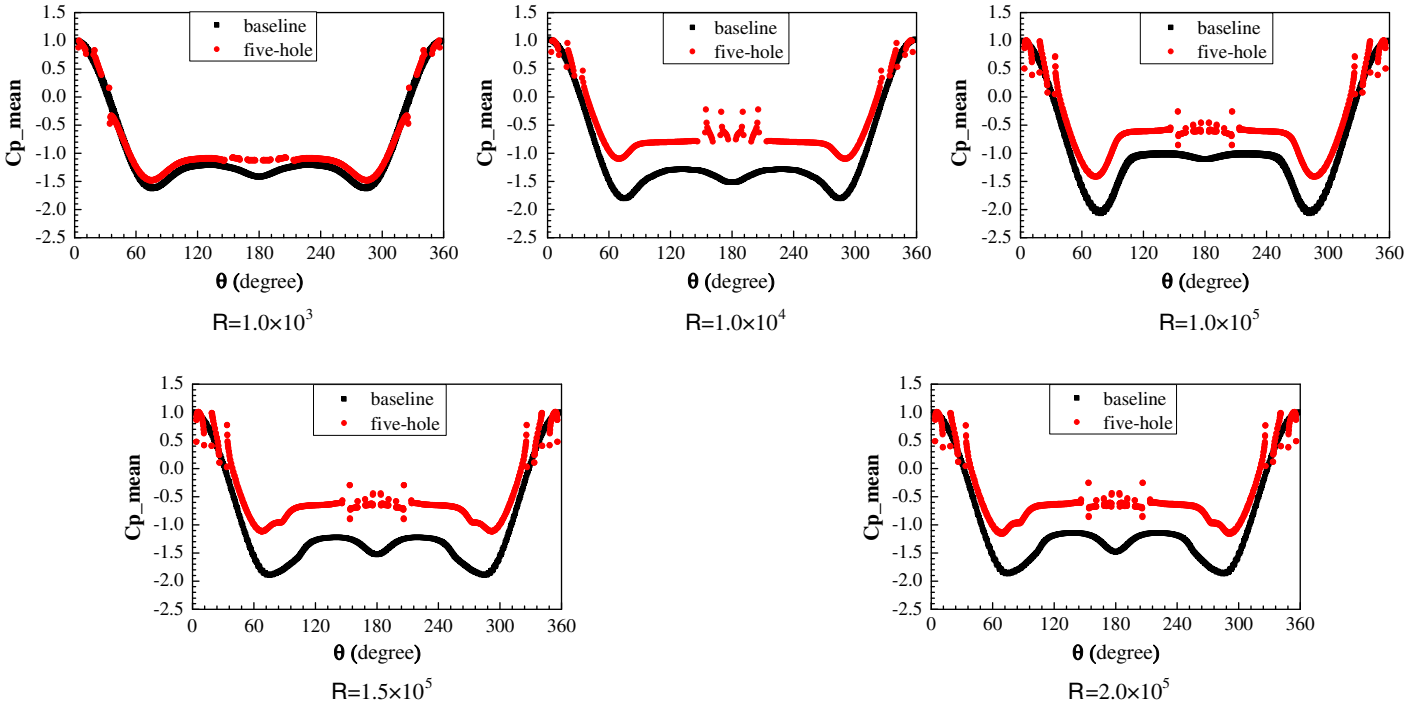

Fig. 4. Mean pressure coefficient on the middle plane of the circular cylinder ($R = 1.0 \times 10^3$ and $R = 1.0 \times 10^5$ reprinted from Chen et al. 2016, with permission of Springer)

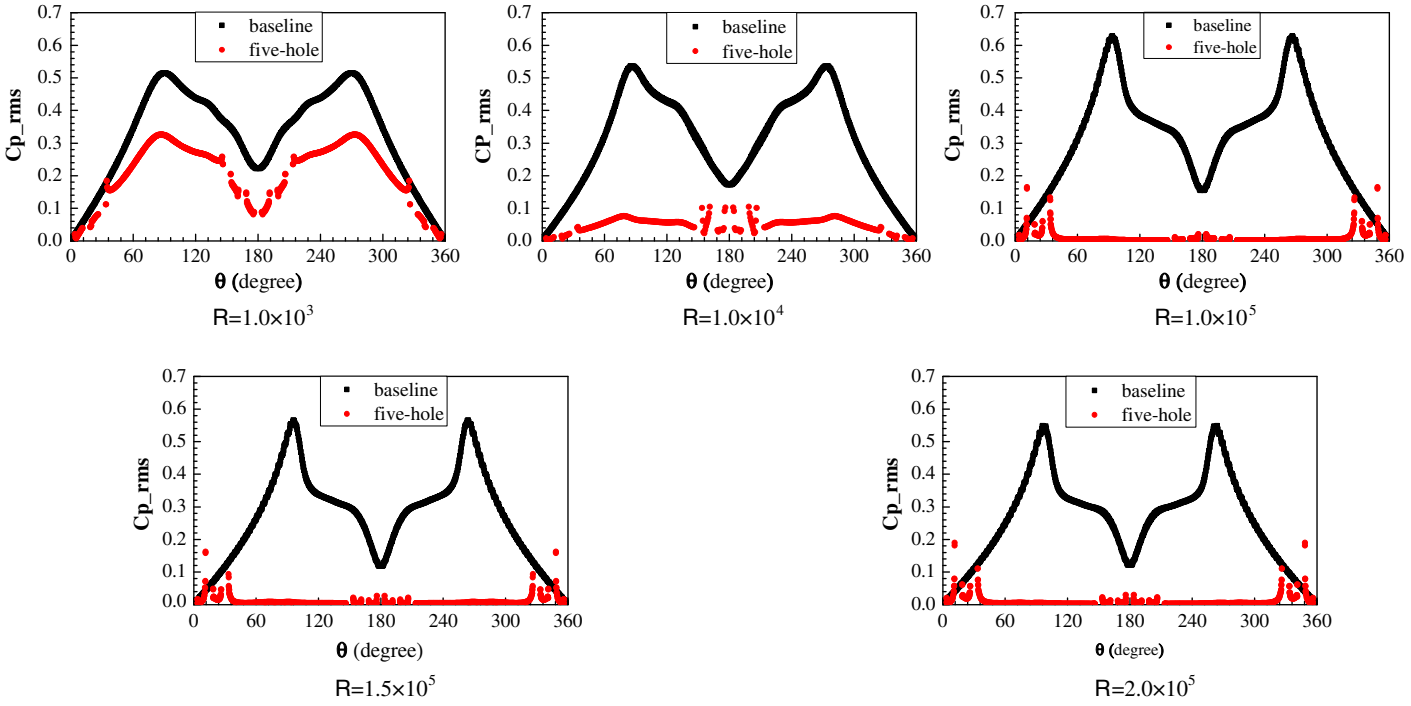

Fig. 5. Fluctuation pressure coefficient on the middle surface of the circular cylinder ($R = 1.0 \times 10^3$ and $R = 1.0 \times 10^5$ reprinted from Chen et al. 2016, with permission of Springer)

RMS values, with a peak value appearing in the region of flow separation. For the five-hole case, the RMS values of the surface pressure coefficients have an enormous decrease and are entirely eliminated when $R \geq 1.0 \times 10^5$. Therefore, it can be revealed that the lift fluctuation of the circular cylinder shows a great reduction for the five-hole case.

Fig. 6 indicates the comparison of the drag and lift coefficient histories between the five-hole case and the baseline result. The aerodynamic coefficients, i.e., lift and drag coefficients, are calculated by integrating the surface pressures around the circular cylinder for the baseline case. However, for the five-hole case, the aerodynamic coefficients are obtained by integrating the surface

Downloaded from ascelibrary.org by Iowa State University on 09/23/22. Copyright ASCE. For personal use only; all rights reserved.

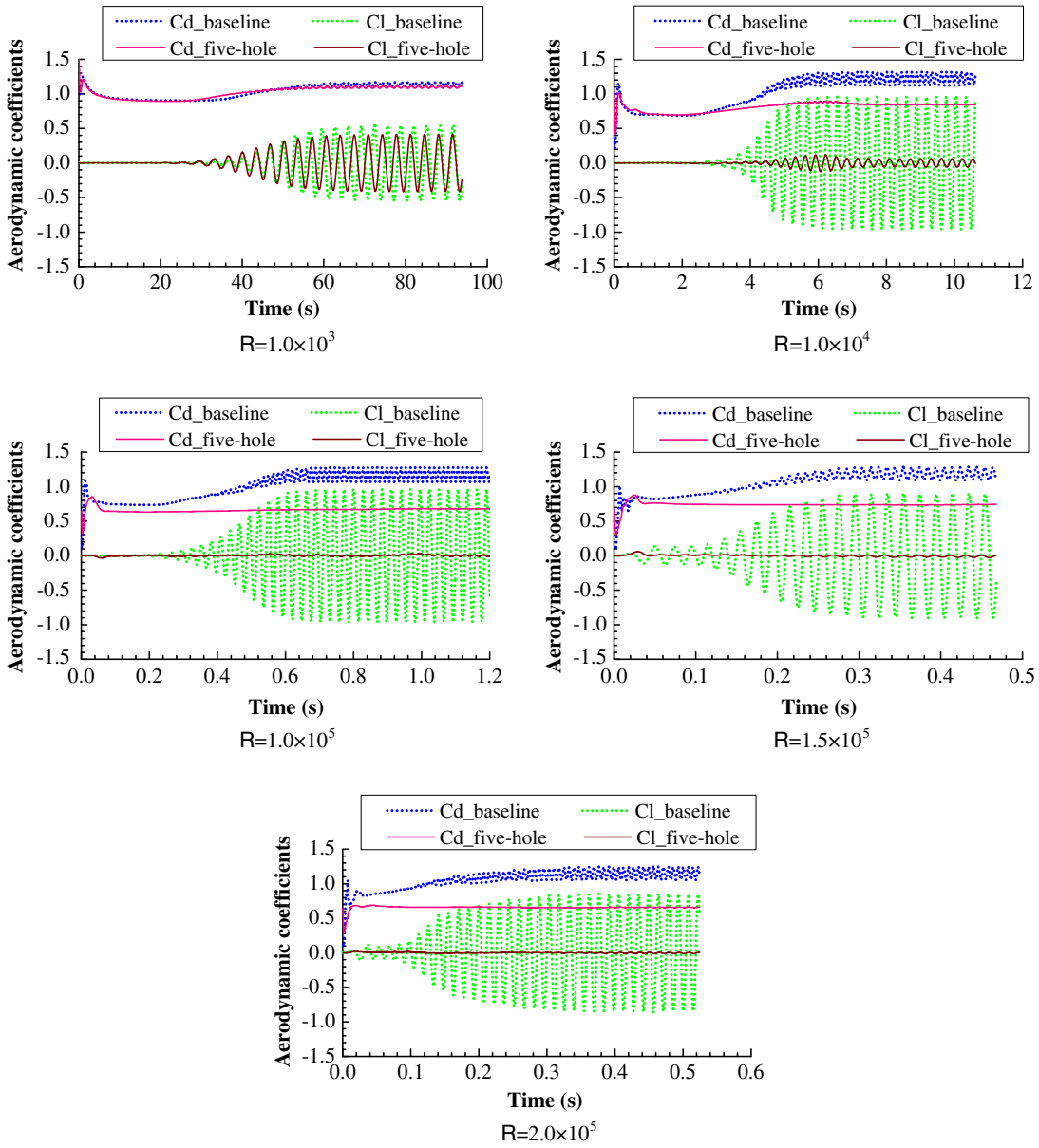

Fig. 6. Time histories of the aerodynamic coefficients

pressure from three surfaces, namely the outer surface, internal surface of the hollow pipe, and the cylinder surface. In comparison with the baseline result, the RMS values of lift coefficients, Cl_{rms}, have been reduced by 23.58, 93.77, 98.44, 98.05, and 99.28% for five different Reynolds numbers, respectively. At the same time, the mean drag coefficients, Cd_{mean}, have been decreased by 3.79, 30.77, 42.43, 37.82, and 43.04%, correspondingly. It is found that the control effects of the drag and lift coefficients are improved by increasing the Reynolds number. When the Reynolds number exceeds 1.0×10^5, the control effects will reach the maximum value: reductions of around 40% and more than 98% for Cd_{mean} and Cl_{rms}, respectively. On the other hand, the control effects are not so remarkable at the low Reynolds numbers (e.g., $R = 1.0 \times 10^3$). As a result, there is still a major component in the frequency spectrum for this Reynolds number and this dominant frequency component disappears at higher Reynolds numbers (e.g., $R = 1.0 \times 10^4 - 2.0 \times 10^5$), as shown in Fig. 7.

The control effectiveness can be quantitatively represented by a nondimensional parameter *Ce*, which is the ratio of the standard deviations or the mean values of the lift or drag coefficients for the five-hole case to the value of the baseline case; for example, $Ce_{\text{-}Cl_{rms}} = (Cl_{\text{-rms-baseline}} - Cl_{\text{-rms-five-hole}})/Cl_{\text{-rms-baseline}}$. If $Ce = 1$, the aerodynamic coefficients drop to zero when the control effectiveness is up to the best value. $Ce = 0$ indicates no control effectiveness. When the aerodynamic coefficient for the five-hole case is larger than the baseline, the control effectiveness is negative, i.e., $Ce < 0$.

Fig. 8 gives the $Ce_{\text{-}Cl_{rms}}$ and $Ce_{\text{-}Cd_{mean}}$ values, which are calculated according to the lift and drag coefficients of the numerical model for the baseline and five-hole cases separately. The simulated results given in Fig. 8 confirm quantitatively that the present passive flow control can reduce the unstable aerodynamic forces of the circular cylinder. Similar to the analysis results of the pressure distribution, the control effects of the lift and drag coefficients are improved with the increase of the Reynolds number and then shows a tendency toward stabilization when $R > 1.0 \times 10^5$.

Figs. 9 and 10 indicate the instantaneous z-swirling strength whose value represents the strength of swirling motion in the *z*-direction around local centers and streamline on the midspan

Downloaded from ascelibrary.org by Iowa State University on 09/23/22. Copyright ASCE. For personal use only; all rights reserved.

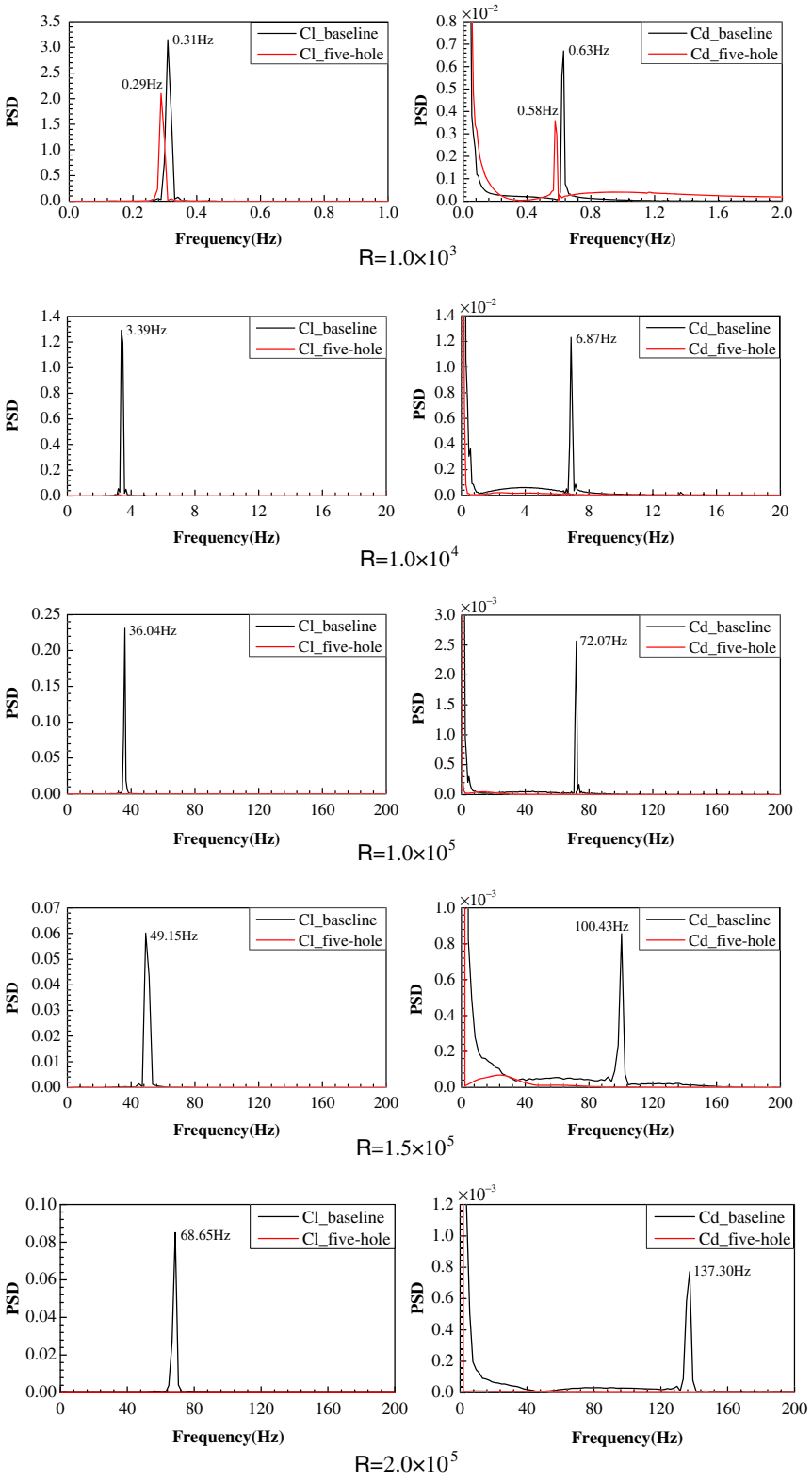

Fig. 7. Comparison of the frequency spectra between the baseline and five-hole cases with different Reynolds numbers

plane when the lift reaches the largest value at different Reynolds numbers, respectively. The wake structures are in the 2 single-vortex (2S) pattern without control while all Reynolds numbers are located in the subcritical region.

The vortices still alternately shed from the surface of the cylinder at the low Reynolds number (i.e., $R = 1.0 \times 10^3$) under control. The air flow from the jet holes did not influence the near wake behind the circular cylinder for the five-hole case. Therefore, there is nearly no change for the pressure distribution of the cylinder compared with the baseline result. The vortex shedding keeps a dominant frequency that is slightly less than that of the baseline case due to its larger diameter. The aerodynamic coefficients acting on the numerical model nearly have no reduction.

J. Aerosp. Eng., 2017, 30(1): 04016063

Downloaded from ascelibrary.org by Iowa State University on 09/23/22. Copyright ASCE. For personal use only; all rights reserved.

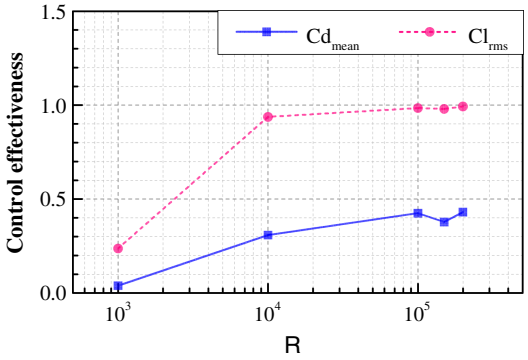

Fig. 8. Control effectiveness of the aerodynamic coefficients in the five-hole case

The flow direction near the jet holes is changed due to the flow blowing effect when $R > 1.0 \times 10^4$. This means that it is difficult to form the main large vortices that appear in the near wake for the baseline case. Moreover, the jet flow from the outlet holes generates a series of small-scale vortices with the opposite direction to the main wake vortex. Therefore, an approximately symmetrical pattern is presented in the near wake for the five-hole controlled case. As a result, the lift fluctuations have been nearly eliminated in comparison with the corresponding baseline result, as shown in Fig. 8. As the fluctuations of aerodynamic forces drop nearly to zero, there are no major frequencies in the frequency spectrum of the aerodynamic force, as shown in Fig. 7.

Fig. 11(a) indicates the time-averaged streamlines between the baseline case and the five-hole controlled case at the high Reynolds number $R = 1.0 \times 10^5$. For the baseline case, a large recirculation region with two reverse vortices forms in the near wake behind the cylinder. However, two pairs of reverse vortices are found to form in the near wake in comparison with two vortices in the far wake for the five-hole case. In each pair of vortices, two inside vortices blowing from the outlet holes are basically fixed and relatively stable. However, two outside vortices shedding from the cylinder develop continuously because of sufficient power being input from the two side wakes. Eventually, the two outside vortices shed alternately behind the two inside vortices, as shown in Fig. 11(b). Because of the vortex shedding being blocked by the two inside vortices and pushed further downstream behind the two inside vortices, the fluctuating pressure on the cylinder surface is reduced greatly. The two inside vortices are regarded as a buffer between the region of the vortex shedding and the cylinder, where the pressure fluctuation decreases dramatically so that the aerodynamic force on the surface of the numerical model drops, especially the lift fluctuation.

Full-Hole Case

The numerical calculations of the full-hole case were finally performed. Figs. 12 and 13 indicate the mean and fluctuating pressure coefficient distributions of the midspan plane of the numerical model, respectively. The results of the full-hole case are similar to those of the five-hole case; however, there exists a small difference at the low Reynolds number of $R = 1.0 \times 10^3$. For the full-hole case, the absolute values of the mean pressure coefficients and the fluctuations of the pressure coefficients in the region of flow separation are larger than the baseline result. This property means that the passive jet flow control method may have negative control effectiveness on the aerodynamic forces. Moreover, because of the full distribution of the suction and jet holes around the numerical model, there exists a relative variation near the holes, regardless of the mean or fluctuating pressure coefficients.

Fig. 14 indicates the compared results of the drag and lift coefficient histories between the full-hole case and the baseline case. In comparison with the baseline result, the mean drag coefficients have been separately reduced by −14.49, 27.24, 39.71, 33.37, and 32.95% at five different Reynolds numbers, respectively. At the same time, the RMS values of lift coefficients have been reduced by −26.84, 88.14, 99.01, 98.14, and 97.07%, as shown in Fig. 15. As mentioned above, for low Reynolds numbers (e.g., $R = 1.0 \times 10^3$), the pressure coefficient fluctuations and the mean pressure coefficients of the cylinder have a slightly increase compared with the baseline result. As a result, this method has a negative control on the lift coefficient fluctuations (−14.49%) and the drag coefficient averages (−26.84%). For other Reynolds numbers (i.e., $R = 1.0 \times 10^4$–2.0×10^5), the control effectiveness of the full-hole case is slightly less than the five-hole result.

Figs. 16 and 17 show the instantaneous streamline and z-swirling on the midspan surface when the lift reaches the largest value for the full-hole case at different Reynolds numbers, respectively. The flow pattern in the near wake behind the circular cylinder for the full-hole case is highly similar to the baseline result at $R = 1.0 \times 10^3$. This means that the full-hole control method has no control effectiveness on the flow pattern at this Reynolds number, or even a small negative control on the flow pattern because there is a so small flux and velocity for the air flow blowing from the jet holes. Thus, the energy injected into the wake is negligible. On the other hand, the fluctuation of the wake will increase because of the obstruction and disturbance of the holes.

The direction of the flow near the jet holes is changed because of the blowing effect in the Reynolds number range of $R = 1.0 \times 10^4 - 2.0 \times 10^5$. This means that it is difficult to form the main large vortices that appear in the near wake for the baseline case. Furthermore, the jet flow from the outlet holes will induce a series of small-scale vortices in the opposite direction of the main wake vortices. The sizes of the reverse vortices generated by the outlet holes of the full-hole case are larger than those of the five-hole case. Similar to the five-hole case, an approximately symmetrical pattern is presented in the near wake under the full-hole jet flow control. As a result, the lift fluctuations have been nearly eliminated in comparison with the baseline result, as shown in Fig. 14.

Fig. 18(a) indicates the comparison result of the time-averaged streamlines between the baseline and the full-hole controlled cases at $R = 1.0 \times 10^5$. Similar to the five-hole case, there are two pairs of reverse vortices in the near wake for the full-hole case. The difference is that two pairs of the vortices (i.e., two inside and two outside vortices) are both basically fixed, not shedding from the cylinder. Behind the two pairs of vortices, there is a large region in which a pair of quite weak vortices appears. It is difficult to observe the periodical vortex shedding, as shown in Fig. 18(b).

The jet momentum coefficient $C\mu$ of the outlet holes denotes the ratio of momentum flux between the jet flow and the incoming free-stream, and is usually employed to characterize the simulated cases with the jet flow control. It is a nondimensional parameter that is defined as $C\mu = A_{\text{out-hole}} u^2_{\text{out-hole}} / A_{\text{oncoming}} u^2_{\text{oncoming}}$, where $A_{\text{out-hole}}$ is the area of all outlet holes, $u_{\text{out-hole}}$ is the average velocity of all outlet holes, A_{oncoming} is the projection area of the control pipe, and u_{oncoming} is the oncoming velocity. Fig. 19 indicates that the jet momentum coefficients change with changes in the Reynolds number for the five-hole case and the full-hole case. The jet momentum coefficient of the five-hole curve is calculated by using five outlet holes [as shown in Fig. 1(a)] for the five-hole case. For the full-hole case, the jet momentum coefficient of the full-hole_full curve is obtained using all outlet holes [the rear half's

Downloaded from ascelibrary.org by Iowa State University on 09/23/22. Copyright ASCE. For personal use only; all rights reserved.

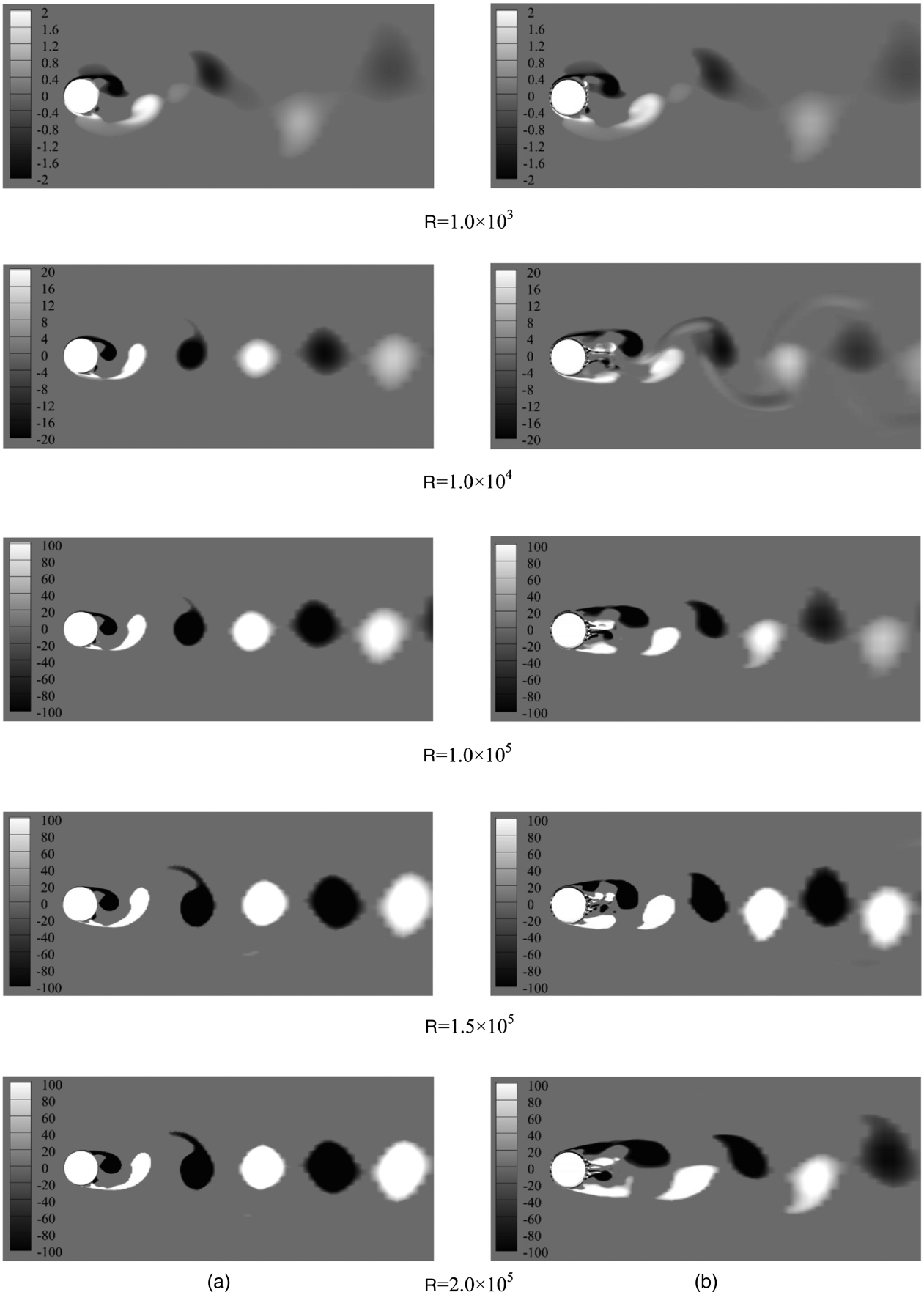

Fig. 9. Z-swirling on the middle surface at the moment of the largest lift: column (a) is the baseline cases; column (b) is the five-hole cases ($R = 1.0 \times 10^3$ and $R = 1.0 \times 10^5$ reprinted from Chen et al. 2016, with permission of Springer)

Downloaded from ascelibrary.org by Iowa State University on 09/23/22. Copyright ASCE. For personal use only; all rights reserved.

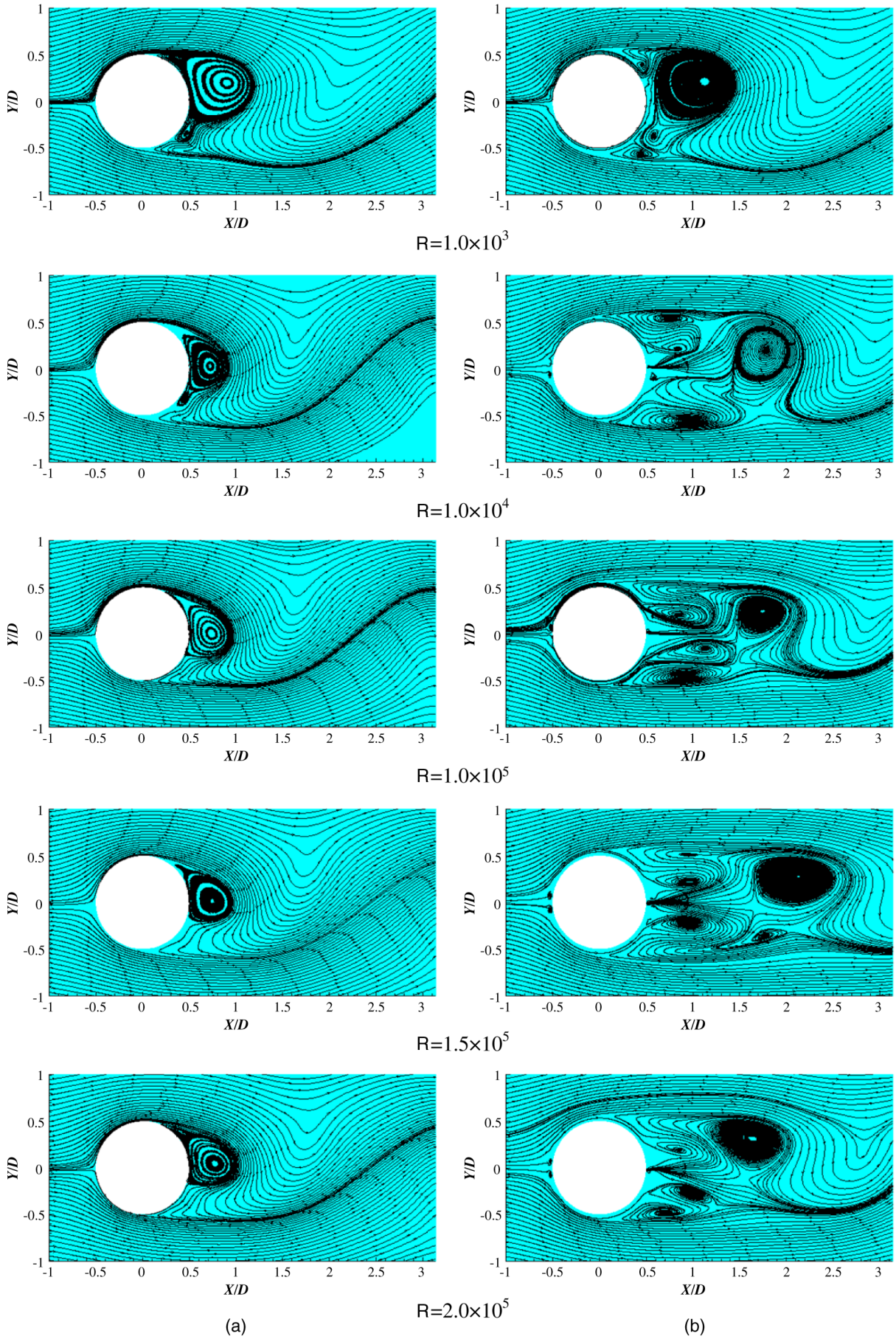

Fig. 10. Streamline on the middle surface at the moment of the largest lift: column (a) is the baseline cases; column (b) is the five-hole cases

Downloaded from ascelibrary.org by Iowa State University on 09/23/22. Copyright ASCE. For personal use only; all rights reserved.

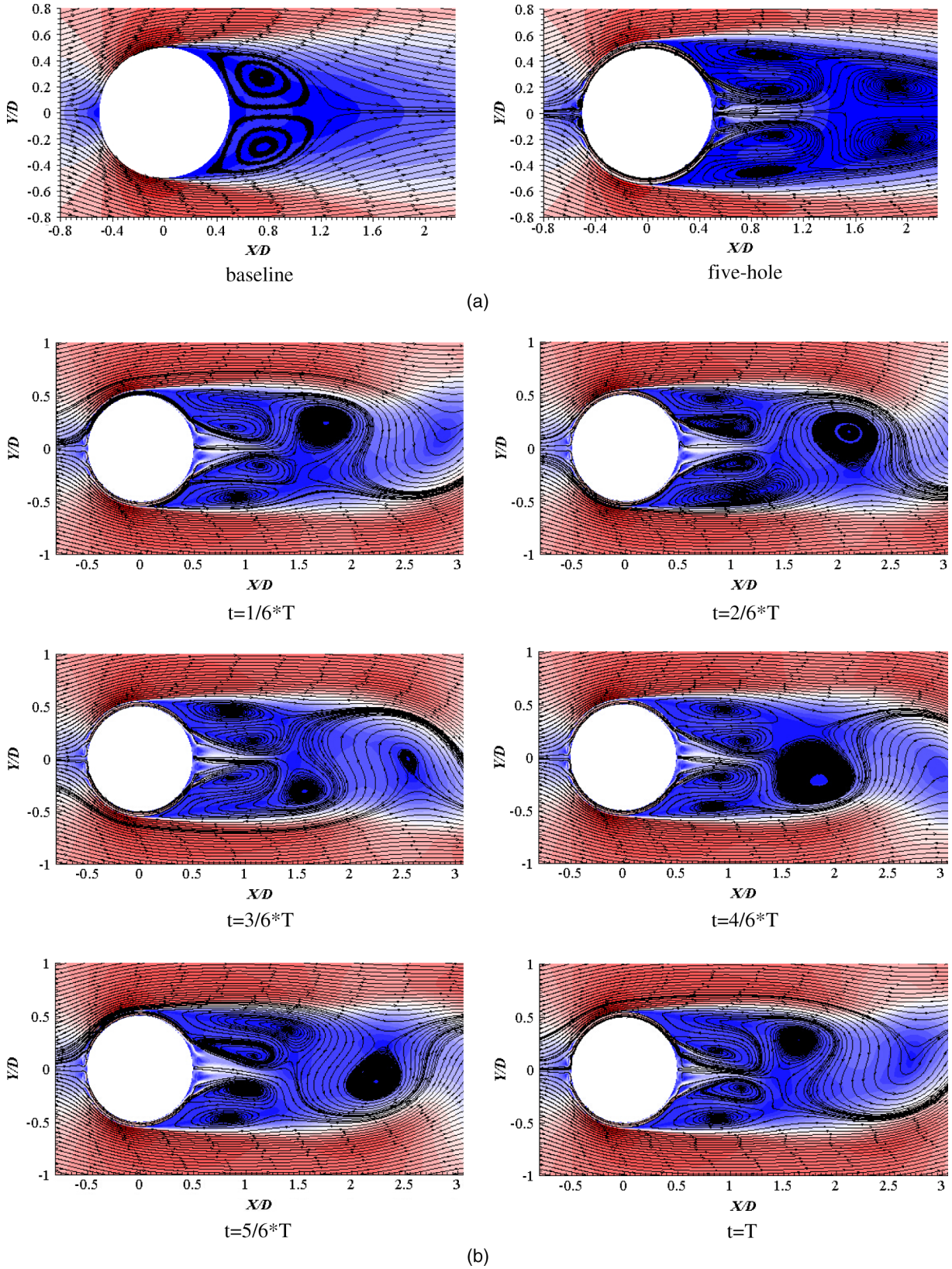

Fig. 11. Streamline in the five-hole case at the Reynolds number $R = 1.0 \times 10^5$: (a) time-averaged streamlines; (b) instantaneous streamline

holes as shown in Fig. 1(a)], and the jet momentum coefficient of the full-hole_five curve is calculated according to five outlet holes in the same locations as those of the five-hole case.

The jet momentum coefficient increases with increments of the Reynolds number, as shown in Fig. 19. Generally, the larger the jet momentum coefficient is, the better the control effective of the jet flow control. In terms of control effectiveness of the aerodynamic coefficients, the five-hole case has slightly better control effectiveness than the full-hole case at higher Reynolds numbers (i.e., exceeding $R = 1.0 \times 10^5$); however, the five-hole results of the jet

Downloaded from ascelibrary.org by Iowa State University on 09/23/22. Copyright ASCE. For personal use only; all rights reserved.

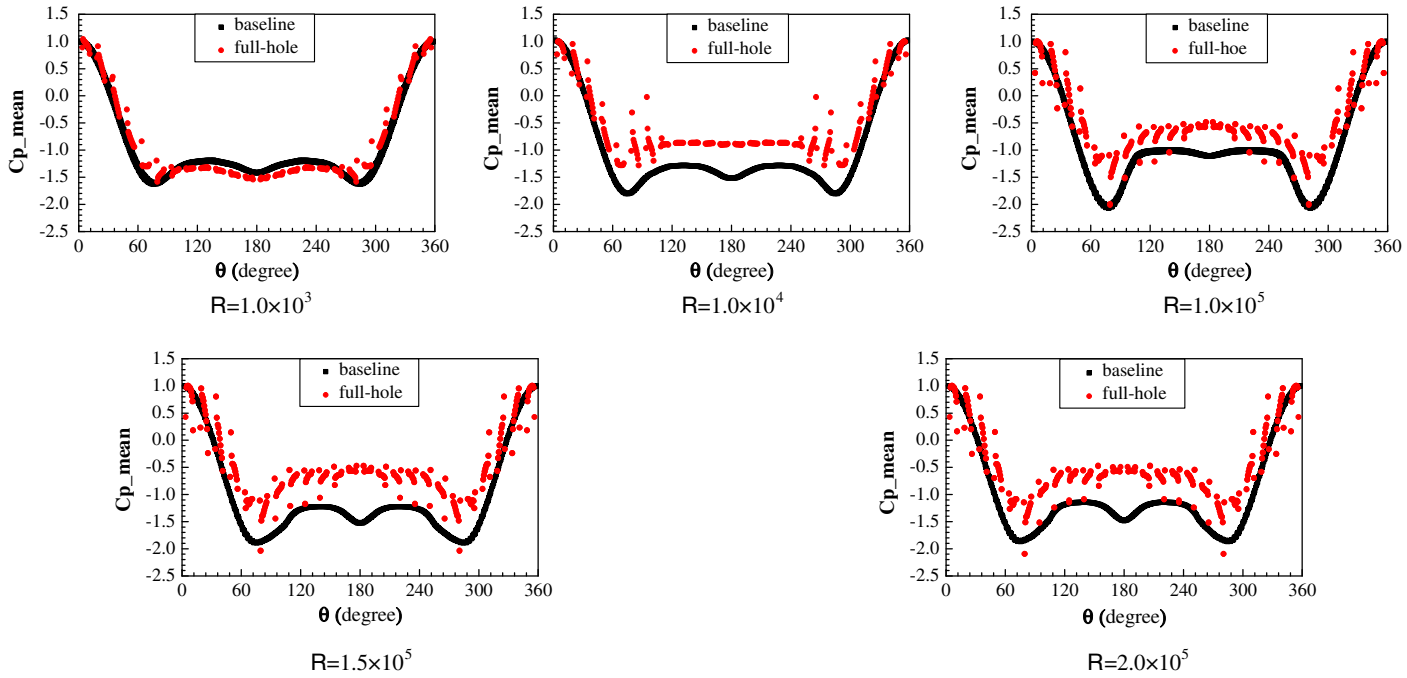

Fig. 12. Mean pressure coefficient on the middle surface of the circular cylinder

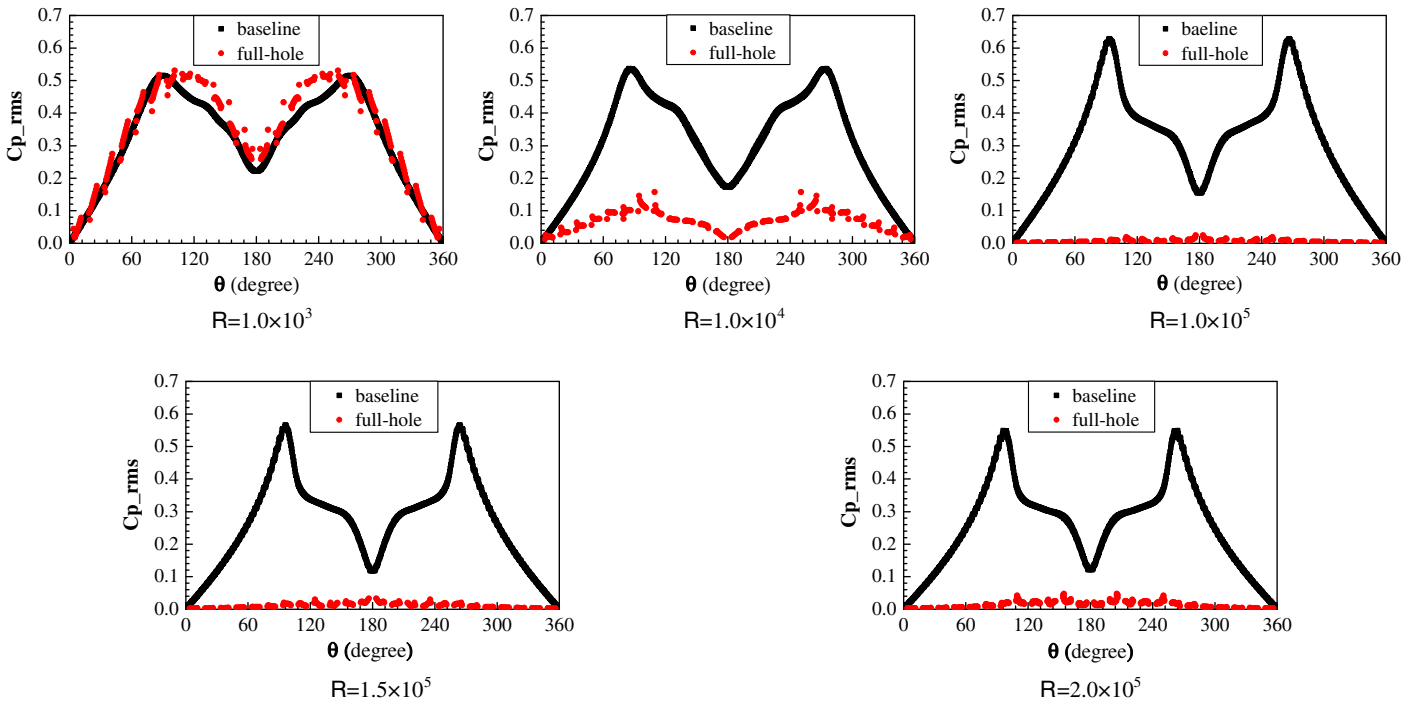

Fig. 13. Fluctuation pressure coefficient on the middle surface of the circular cylinder

momentum coefficients are less than those of the full-hole_full curve and larger than those of the full-hole_five curve. It is indicated that the locations of the outlet holes (i.e., jet holes) are also important to the control effectiveness. Although the full-hole_five curve is lower than the five-hole curve, the full-hole case can obtain the same level of control effectiveness when the angle of attack of the oncoming flow changes. The full-hole case is more applicable than the five-hole case in practical engineering.

Stability Analysis

The absolute instability of the wake behind the circular cylinder is responsible for the vortex streets behind stationary cylinders. According to the linear stability theory, solving the Orr-Sommerfeld equation can determine if the velocity profile is stable or unstable. Then the absolute instability region of uncontrolled and controlled cases can be discussed. If the absolute instability region behind the

Downloaded from ascelibrary.org by Iowa State University on 09/23/22. Copyright ASCE. For personal use only; all rights reserved.

Downloaded from ascelibrary.org by Iowa State University on 09/23/22. Copyright ASCE. For personal use only; all rights reserved.

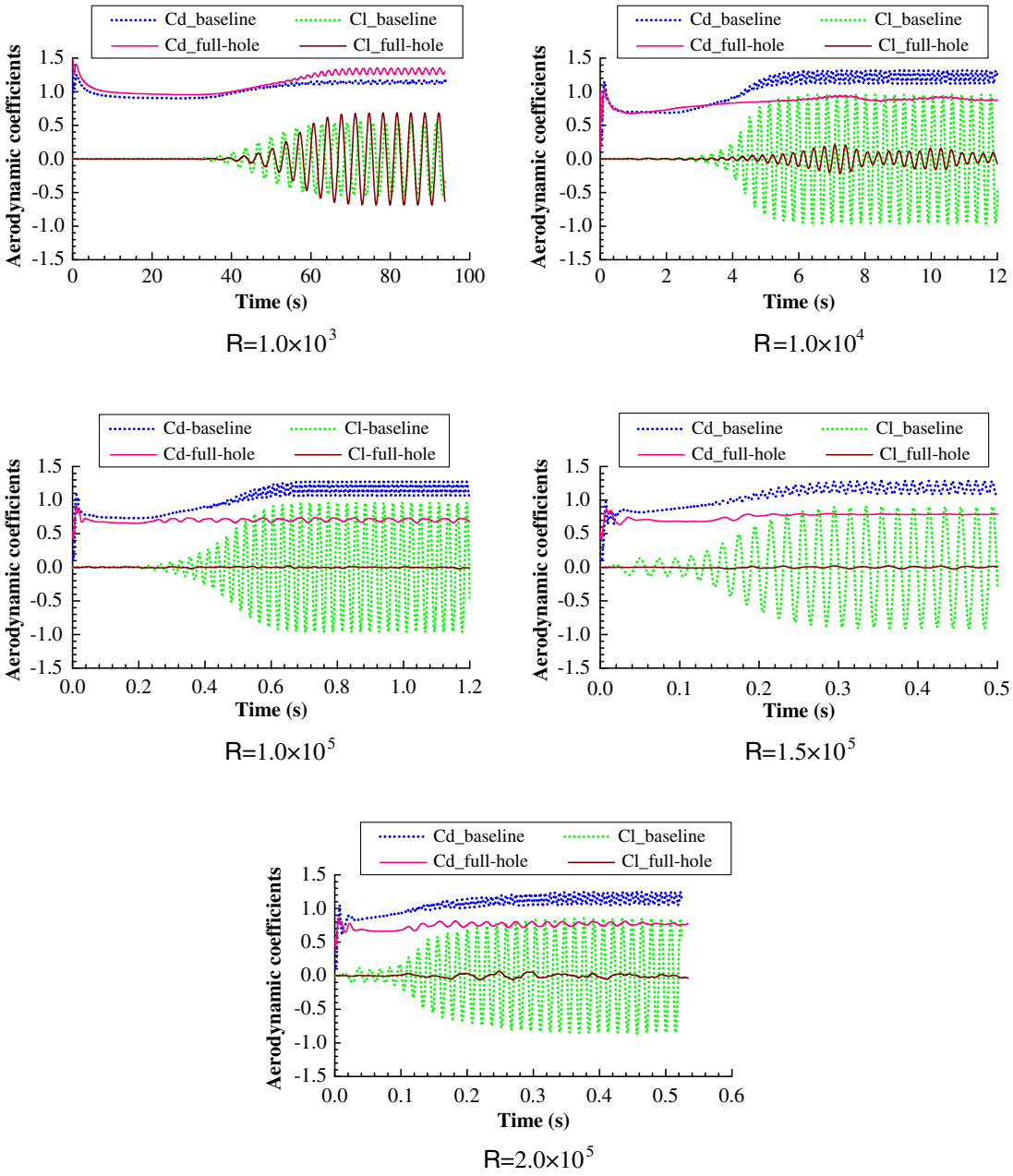

Fig. 14. Time history curves of the aerodynamic coefficient

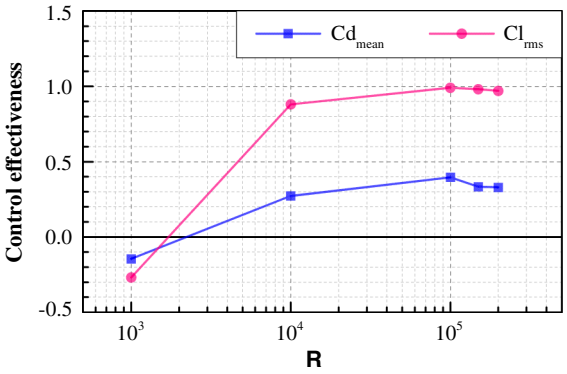

Fig. 15. Control effectiveness of the aerodynamic coefficients in the full-hole cases

cylinder shrinks or even disappears in controlled cases, the vortex formation or shedding mode in the wake might witness a change.

As for two-dimensional parallel shear flow, the average velocity U is just related to the coordinate Y. There is a disturbance stream-function $\psi(x, y, t)$. In order to satisfy the continuity equation, it is assumed that

$$\psi(x, y, t) = \phi(y)e^{i(\alpha x - \omega t)} \tag{1}$$

$$u'(x, y, t) = \frac{\partial \psi}{\partial y} \tag{2}$$

$$v'(x, y, t) = -\frac{\partial \psi}{\partial x} \tag{3}$$

where α = complex wave number; β = complex frequency; and u' and v' = disturbance velocity in x-direction and y-direction

Downloaded from ascelibrary.org by Iowa State University on 09/23/22. Copyright ASCE. For personal use only; all rights reserved.

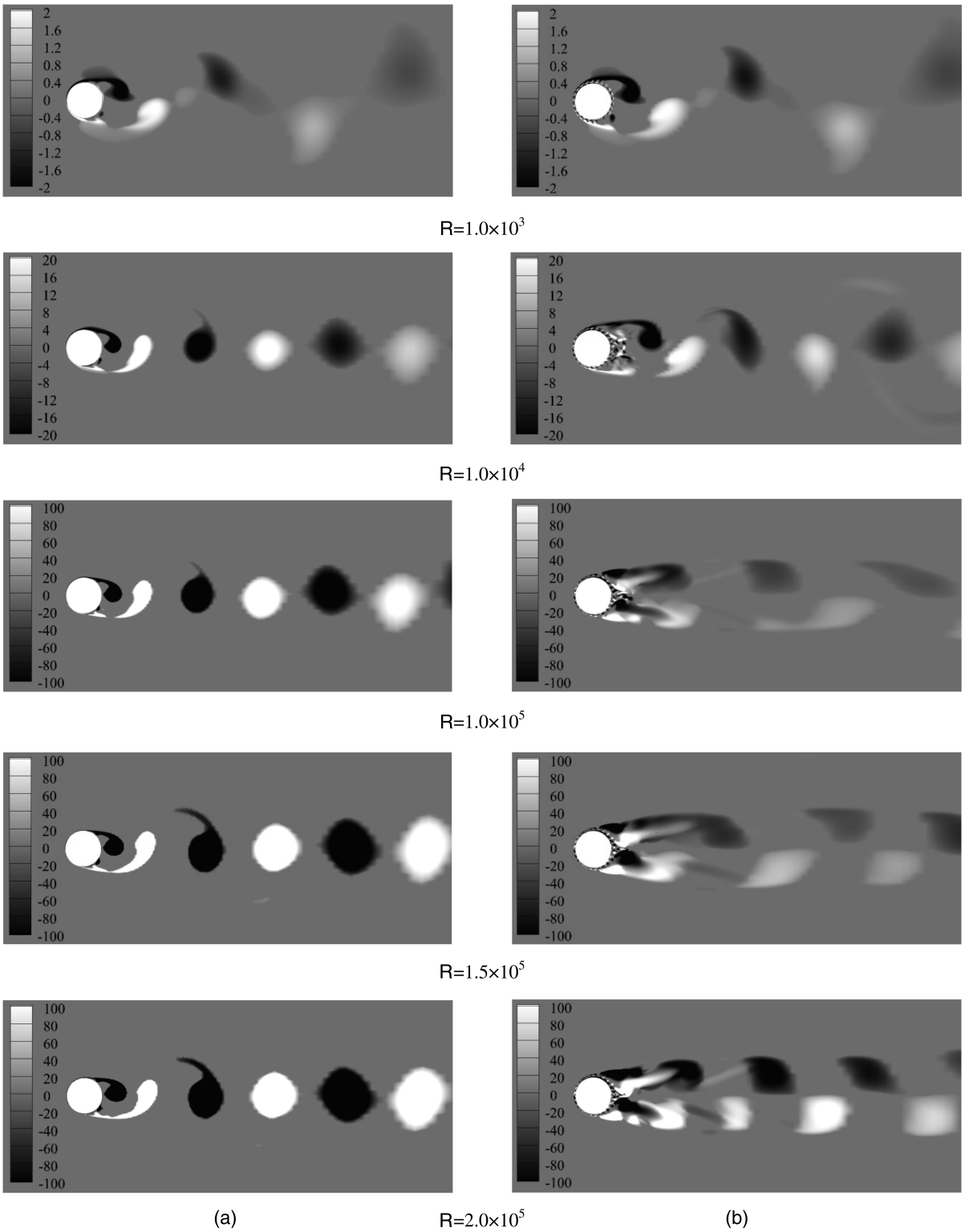

Fig. 16. Z-swirling on the middle surface at the moment of the largest lift: column (a) is the baseline cases; column (b) is the full-hole cases

components separately. Thus, $\phi(y)$ satisfies Orr-Sommerfeld equation of incompressible flow

$$\left(\bar{U}\text{-}\frac{\omega}{\alpha}\right)(\phi'' - \alpha^2 l^2 \phi) - \bar{U}''\phi = -\frac{i}{\alpha l \cdot \mathrm{R}}(\phi'''' - 2\alpha^2 l^2 \phi'' + \alpha^4 l^4 \phi) \tag{4}$$

where $\bar{U} = U/U_\infty$; U_∞ = reference velocity; l = reference length (diameter of the cylinder usually); R Reynolds number, corresponding to the reference velocity and length. If the effect of viscosity is not taken into consideration, the Orr-Sommerfeld equation of inviscid and incompressible flow is

$$\alpha\bar{U}(\phi'' - \alpha^2 l^2 \phi) - \alpha\bar{U}''\phi = \omega(\phi'' - \alpha^2 l^2 \phi) \tag{5}$$

Orszag (1971) used the expansions in Chebyshev polynomials to solve the Orr-Sommerfeld equation approximately, which yielded very satisfactory results. The explanation why expansions

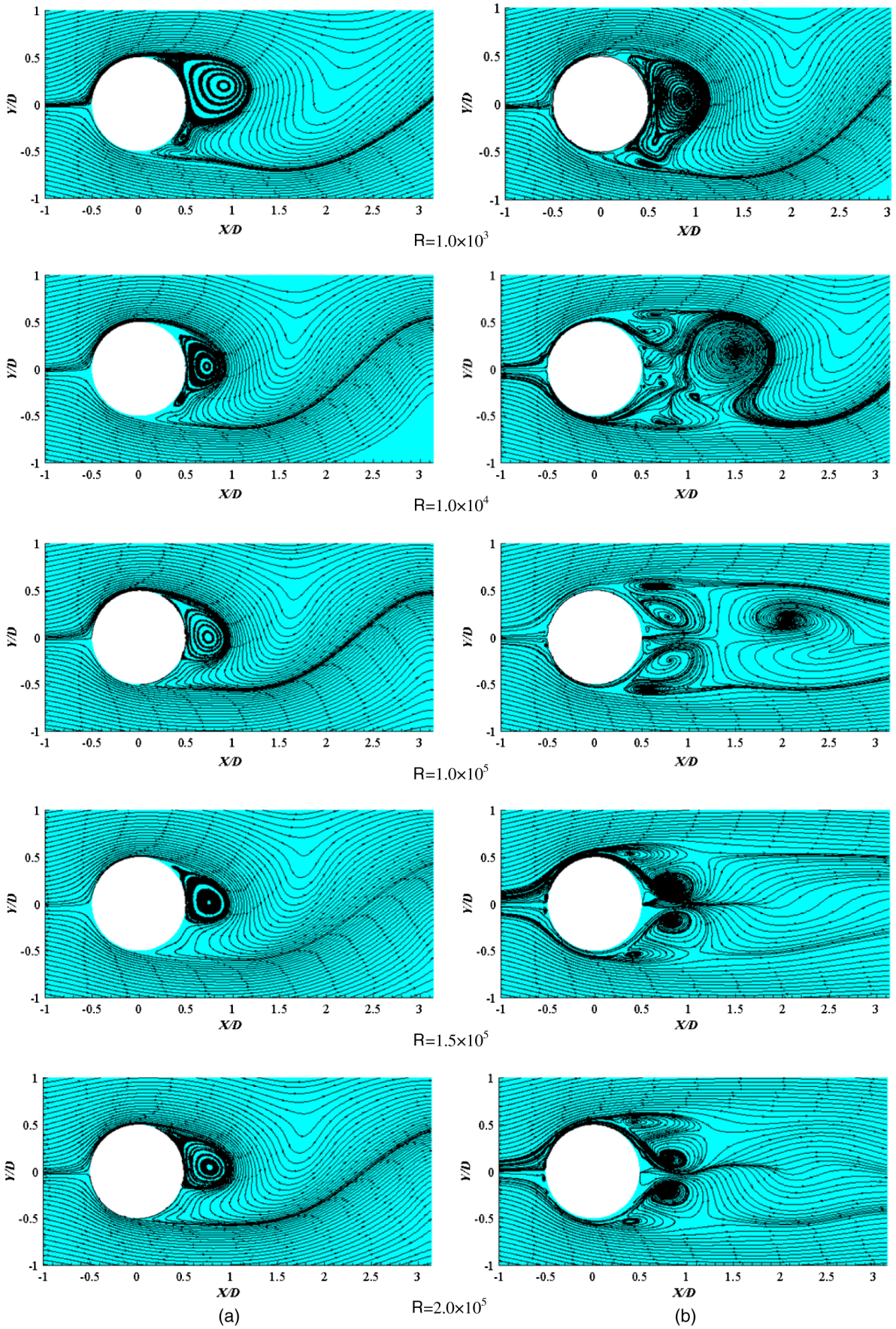

Fig. 17. Streamline on the middle surface at the moment of the largest lift: column (a) is the baseline cases; column (b) is the full-hole cases

Downloaded from ascelibrary.org by Iowa State University on 09/23/22. Copyright ASCE. For personal use only; all rights reserved.

in Chebyshev polynomials are superior to the expansions in other also had been given.

As for the wake behind the cylinder, the boundary conditions are

$$u'(x, \pm\infty, t) = 0 \tag{6}$$

$$v'(x, \pm\infty, t) = 0 \tag{7}$$

If the disturbance stream-function $\psi(x, y, t)$ is symmetric relative to the coordinate Y, where the wake vortex stand in one line, the expansion coefficients in Chebyshev polynomials are even numbers, for example

$$\phi(y) = \sum_{n=0}^{+\infty} a_n T_n(y) \quad n = 0, 2, 4, 6, \ldots \tag{8}$$

If the disturbance stream-function $\psi(x, y, t)$ is antisymmetric, relative to the coordinate Y, where the wake vortex stand in two parallel line, the expansion coefficients in Chebyshev polynomials are odd numbers, for example

$$\phi(y) = \sum_{n=1}^{+\infty} a_n T_n(y) \quad n = 1, 3, 5, 7, \ldots \tag{9}$$

where $T_n(y)$ = Chebyshev polynomial $T_n(y) = \cos(n \arccos y)$.

Then, the Orr-Sommerfeld equation of inviscid and incompressible flow can be expressed as the following matrix form:

$$(A - \omega B)\phi = 0 \tag{10}$$

The matrices A and B are just related with the complex wave number α. According to the dispersion relation $|A - \omega B| = 0$, a double root of the dispersion relation can be found. That is to say the group velocity is equal to zero: $\partial\omega(\alpha_0)/\partial\alpha = 0$. If the imaginary part $\omega_i(\alpha_0)$ of the complex frequency $\omega(\alpha_0)$ is positive, the local disturbance is absolute instability. Or, it is a convective instability.

The temporal average velocity profiles at different x stations have been extracted for baseline cases and controlled cases. Fig. 20 gives some representative velocity profiles at $\mathrm{R} = 10^3$ and $\mathrm{R} = 10^5$. At the low Reynolds number, the velocity profiles of the three cases are quite similar. However, there is substantial recovery in the intermediate region for controlled cases at high Reynolds numbers. The double root point, called critical point, can be found through mapping the rectangular grid in the α- plane to its image in the ω- plane via the dispersion relation, as shown in Fig. 21. The value of ω_i at the critical point seems not to go down at Reynolds number $\mathrm{R} = 10^3$. The absolute instability region behind the cylinder experiences no shrinkage when the x station moves far away from the circular cylinder. Fig. 22(a) shows that the value of ω_i at the critical point for the full-hole case is larger than that of the baseline, which is in agreement with aerodynamic force of the cylinder. At Reynolds number $\mathrm{R} = 10^5$, the ω_i at the critical point decreases substantially for controlled cases. The absolute instability region near the cylinder shrinks substantially for the full-hole case. Particularly, the absolute instability region disappears in the very wake of the cylinder for the five-hole case, as shown in Fig. 22(b). The velocity profiles behind the cylinder have a great change because of the influence of the jet flow from the outlet holes at a high Reynolds number. The absolute instability in the wake is destroyed so that the alternate shedding vortex cannot develop.

Conclusions

A passive suction/jet flow control method has been presented to manipulate the alternating vortex shedding behind a circular cylinder based on a numerical calculation in the paper. The idea originates from active blowing/suction control methods and is applied to passive control methods, which imparts the advantages of both the active blowing/suction control methods and the passive control methods: good control effectiveness and no active energy injection requirements.

In the current paper, the baseline, five-hole, and full-hole cases are analyzed at the Reynolds numbers of 1.0×10^3, 1.0×10^4, 1.0×10^5, 1.5×10^5, and 2.0×10^5. Some conclusions are obtained as follows:

1. For the Reynolds number across almost the entirety of the subcritical region (wind speed from 0.146 to 29.215 m/s), a better control effectiveness appears at a higher Reynolds number $\mathrm{R} > 1.0 \times 10^4$. When $\mathrm{R} > 1.0 \times 10^5$, the control effectiveness of the passive suction/jet flow control method will maintain the maximum value. However, there is nearly no change of the aerodynamic force at the low Reynolds numbers (e.g., $\mathrm{R} = 1.0 \times 10^3$). The absolute instability region shrinks or even disappears in the very close region near the cylinder for controlled cases.
2. The control effectiveness of the lift coefficient is superior to the drag coefficient result. The cross-flow lift force has been basically eliminated when $\mathrm{R} > 1.0 \times 10^5$. The largest reductions

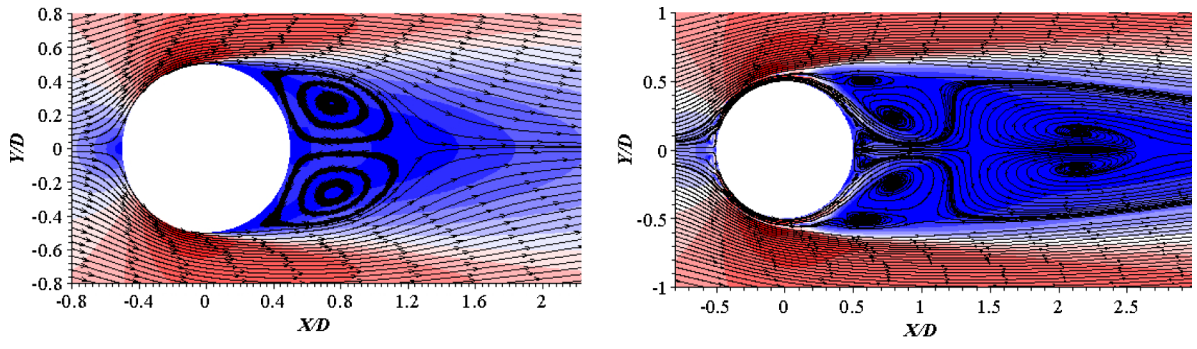

Fig. 18. Streamline in full-hole case at the Reynolds number $\mathrm{R} = 1.0 \times 10^5$: (a) time-averaged streamlines; (b) instantaneous streamline

Downloaded from ascelibrary.org by Iowa State University on 09/23/22. Copyright ASCE. For personal use only; all rights reserved.

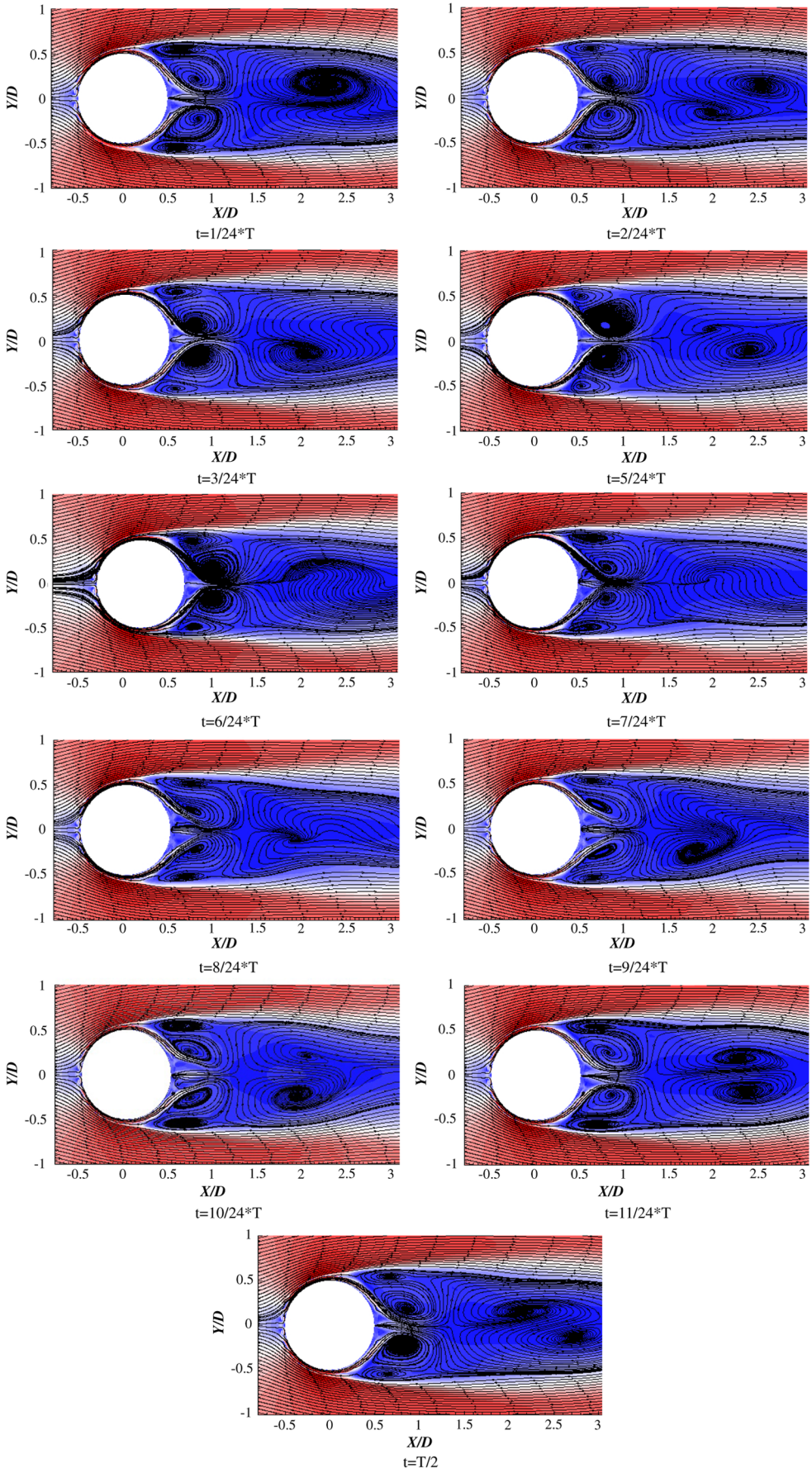

(b)

Fig. 18. (*Continued.*)

Downloaded from ascelibrary.org by Iowa State University on 09/23/22. Copyright ASCE. For personal use only; all rights reserved.

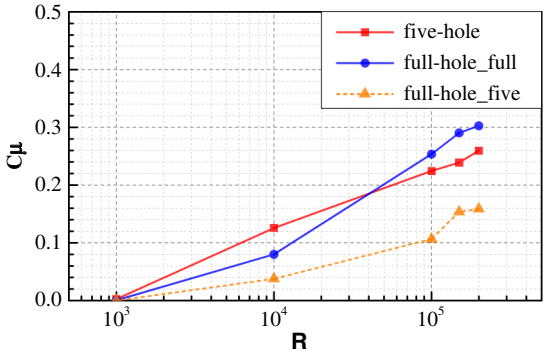

Fig. 19. Comparison of the jet momentum coefficient between the five-hole case and the full-hole case

were, separately, by 99.28 and 99.01% for Cl_{rms} for the five-hole and full-hole cases, respectively; however, the reductions are 43.04 and 39.71% for Cd_{mean} for the five-hole and full-hole cases, respectively.

3. The control effectiveness of the five-hole case is slightly better than the full-hole case result. However, one must take into consideration that the oncoming flow direction needs to be known in advance and is fixed for the five-hole case, making it difficult to achieve these requirements. Therefore, the full-hole case has a better practical significance.

In practical engineering, the Reynolds number is often notably high. Thus, this method can play an important role in suppressing unsteady vortex shedding from circular cylinders, such as the stay cable, suspension cable, electric wire, even marine riser, etc. However, the size and space of the holes are not investigated in the

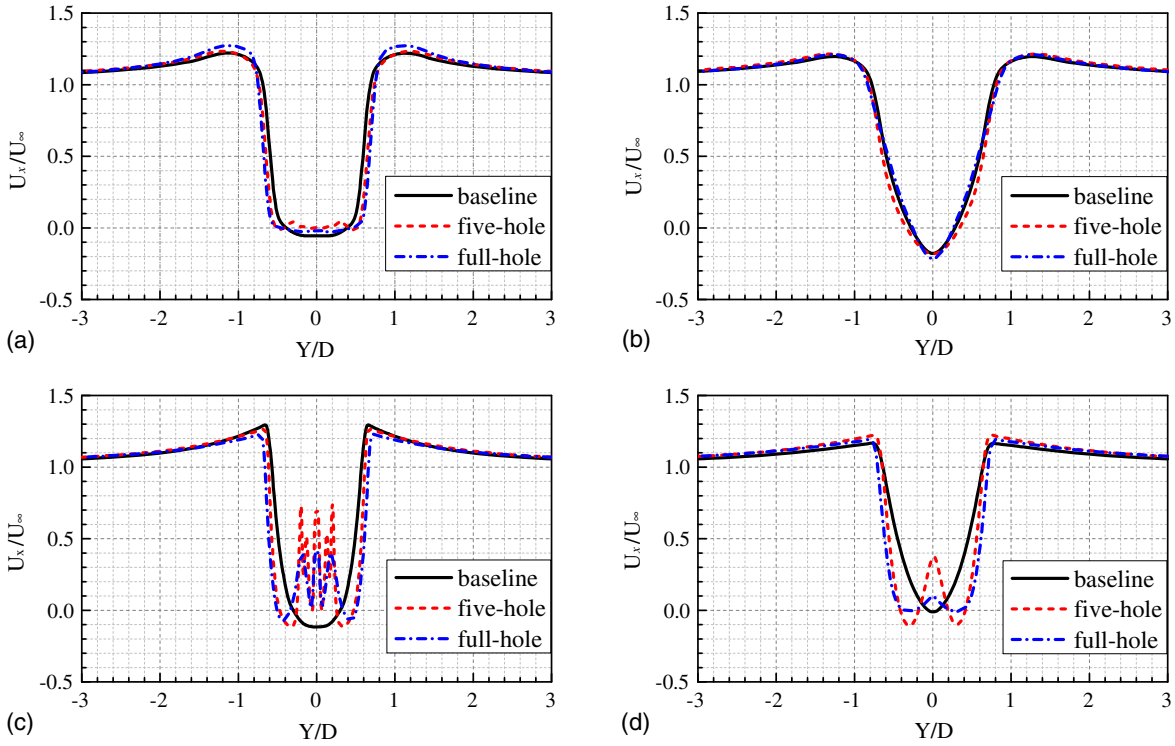

Fig. 20. Velocity profile at different x stations: (a) $x/d = 0.6$, $R = 10^3$; (b) $x/d = 1.2$, $R = 10^3$; (c) $x/d = 0.6$, $R = 10^5$; (d) $x/d = 1.2$, $R = 10^5$

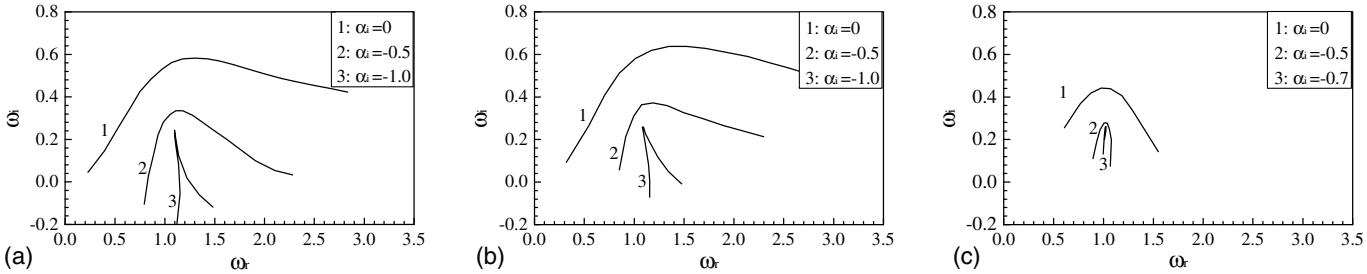

Fig. 21. Map of lines α_i = constant in the ω-plane at $x/d = 1.2$ for $R = 10^3$: (a) baseline; (b) five-hole; (c) full-hole

Downloaded from ascelibrary.org by Iowa State University on 09/23/22. Copyright ASCE. For personal use only; all rights reserved.

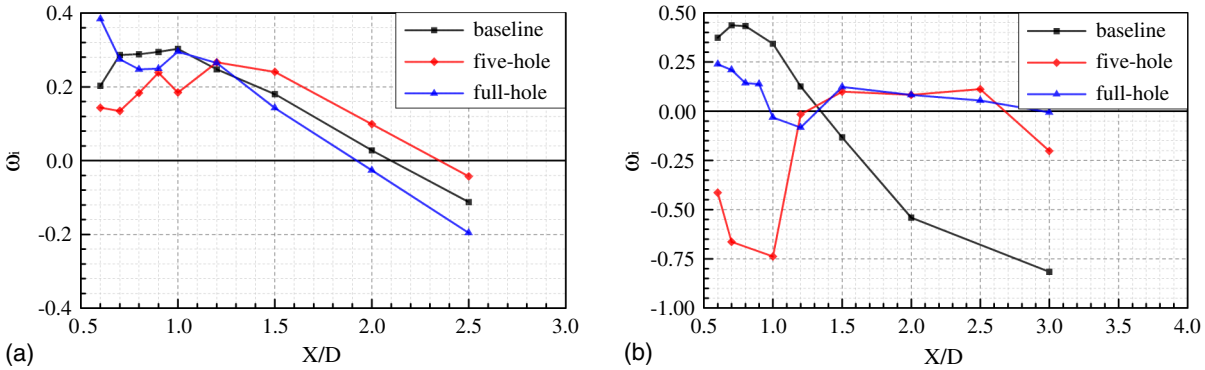

Fig. 22. ω_i in the critical point versus x/d: (a) $R = 10^3$; (b) $R = 10^5$

present paper, which may have a great influence on the control effectiveness. In future work, it is necessary to discuss the influence of these parameters quantitatively to select an optimal scheme.

Acknowledgments

This research was funded by the National Natural Sciences Foundation of China (NSFC) (51378153, 51008093, 51161120359, and 91215302).

References

Al-Jamal, H., and Dalton, C. (2004). "Vortex induced vibrations using large eddy simulation at a moderate Reynolds number." *J. Fluids Struct.*, 19(1), 73–92.

Anderson, E. A., and Szewczyk, A. A. (1997). "Effects of a splitter plate on the near wake of a circular cylinder in 2 and 3-dimensional flow configurations." *Exp. Fluids*, 23(2), 161–174.

ANSYS FLUENT 14.5 [Computer software]. Ansys, Canonsburg, PA.

Arcas, D. R., and Redekopp, L. G. (2004). "Aspects of wake vortex control through base blowing/ suction." *Phys. Fluids*, 16(2), 452–456.

Bearman, P. W. (1969). "On vortex shedding from a circular cylinder in the critical Reynolds number regime." *J. Fluid Mech.*, 37(3), 577–585.

Bearman, P. W., and Harvey, J. K. (1993). "Control of circular cylinder flow by the use of dimples." *AIAA J.*, 31(10), 1753–1756.

Blevins, R. D. (1990). *Flow-induced vibration*, 2nd Ed., Van Nostrand Reinhold, New York.

Breuer, M. (2000). "A challenging test case for large eddy simulation: High Reynolds number circular cylinder flow." *Int. J. Heat Fluid Flow*, 21(5), 648–654.

Chen, W. L., Li, H., and Hu, H. (2014). "An experimental study on a suction flow control method to reduce the unsteadiness of the wind loads acting on a circular cylinder." *Exp. Fluids*, 55(1707), 1–20.

Chen, W. L., Wang, X. J., Xu, F., Li, H., and Hu, H. (2016). "Numerical simulation study on a passive jet flow control method to suppress unsteady vortex shedding from a circular cylinder." *Fluid-Structure-Sound Interactions and Control*, Springer, Berlin, 441–446.

Chen, W. L., Xin, D. B., Xu, F., Li, H., Ou, J. P., and Hu, H. (2013). "Suppression of vortex-induced vibration of a circular cylinder using suction-based flow control." *J. Fluids Struct.*, 42, 25–39.

Delany, N. K., and Sorensen, N. E. (1953). "Low-speed drag of cylinders of various shapes." *Technical Note 303*, National Advisory Committee for Aeronautics, Washington.

Drescher, H. (1956). "Messung der auf querangeströmte Zylinder ausgeübten zeitlich veränderten Drücke." *Zeitschrift für Flugwissenschaften und Weltraumforschung*, 4(1/2), 17–21 (in German).

Favier, J., Dauptain, A., Basso, D., and Bottaro, A. (2009). "Passive separation control using a self-adaptive hairy coating." *J. Fluid Mech.*, 627, 451–483.

Feng, L. H., and Wang, J. J. (2010). "Circular cylinder wake vortex synchronization control with synthetic jet positioned at back stagnation point." *J. Fluid Mech.*, 662, 232–259.

Feng, L. H., and Wang, J. J. (2012). "Synthetic jet control of separation in the flow over a circular cylinder." *Exp. Fluids*, 53(2), 467–480.

Feng, L. H., Wang, J. J., and Pan, C. (2010). "Effect of novel synthetic jet on wake vortex shedding modes of a circular cylinder." *J. Fluids Struct.*, 26(6), 900–917.

Feng, L. H., Wang, J. J., and Pan, C. (2011). "Proper orthogonal decomposition analysis of vortex dynamics of a circular cylinder under synthetic jet control." *Phys. Fluid*, 23(1), 014106-1–014106-113.

Gartshore, I. S. (1984). "Some effects of upstream turbulence on the unsteady lift forces imposed on prismatic two dimensional bodies." *J. Fluids Eng.*, 106(4), 418–424.

Keefe, R. T. (1962). "Investigation of the fluctuating forces acting on a stationary circular cylinder in a subsonic stream and of the associated sound field." *J. Acoust. Soc. Am.*, 34(11), 1711–1714.

Labbe, D. F. L., and Wilson, P. A. (2007). "A numerical investigation of the effects of the spanwise length on the 3-D wake of a circular cylinder." *J. Fluids Struct.*, 23(8), 1168–1188.

Lee, S. J., and Kim, H. B. (1997). "The effect of surface protrusions on the near wake of a circular cylinder." *J. Wind Eng. Ind. Aerodyn.*, 69–71, 351–361.

Leehey, P., and Hanson, C. E. (1971). "Aeolian tones associated with resonant vibration." *J. Sound Vib.*, 13(4), 465–483.

Lim, H. C., and Lee, S. J. (2002). "Flow control of circular cylinders with longitudinal grooved surfaces." *AIAA J.*, 40(10), 2027–2036.

Moeller, M. J., and Leehey, P. (1984). "Unsteady forces on a cylinder in cross flow at subcritical Reynolds numbers." *ASME Symp. on Flow-Induced Vibrations*, M. P. Païdoussis, O. M. Griffin, and M. Sevik, eds., Vol. 1, ASME, New York, 57–71.

Mohr, K. H. (1981). "Messungen instationären Drücke bei Queranströmung von Kreiszylindern unter Berücksichtigung fluidelastischer Effekte." Ph.D. thesis, KFA Jülich GmbH, Germany.

Morkovin, M. V. (1964). "Flow around circular cylinder—A kaleidoscope of challenging fluid phenomena." *ASME Symp. on Fully Separated Flows*, ASME, Philadelphia, 102–118.

Munson, B. R., Young, F. D., and Okiis, T. H. (2002). *Fundamentals of fluid mechanics*, 5th Ed., Wiley, New Delhi, India.

Norberg, C. (1994). "An experimental investigation of the flow around a circular cylinder: Influence of aspect ratio." *J. Fluid Mech.*, 258, 287–316.

Norberg, C. (2003). "Fluctuating lift on a circular cylinder: Review and new measurements." *J. Fluids Struct.*, 17(1), 57–96.

Orszag, S. A. (1971). "Accurate solution of the Orr-Sommerfeld stability equation." *J. Fluid Mech.*, 50(04), 689–703.

Relf, E. F., and Simmons, E. F. G. (1924). *The frequency of eddies generated by the motion of circular cylinders through a fluid*, Taylor & Francis, Abingdon, U.K.

Downloaded from ascelibrary.org by Iowa State University on 09/23/22. Copyright ASCE. For personal use only; all rights reserved.

Ribeiro, J. L. D. (1992). "Fluctuating lift and its spanwise correlation on a circular cylinder in a smooth and in a turbulent flow: A critical review." *J. Wind Eng. Ind. Aerodyn.*, 40(2), 179–198.

Ribner, H. S., and Etkin, B. (1958). "Noise research in Canada." *Proc., 1st International Congress of the Aeronautical Sciences*, Pergamon Press, London.

Roshko, A. (1961). "Experiments on the flow past a circular cylinder at very high Reynolds number." *J. Fluid Mech.*, 10(03), 345–356.

Sakamoto, H., and Haniu, H. (1994). "Optimum suppression of fluid forces acting on a circular cylinder." *J. Fluids Eng.*, 116(2), 221–227.

Shih, W. C. L., Wang, C., Coles, D., and Roshko, A. (1993). "Experiments on flow past rough circular cylinders at large Reynolds numbers." *J. Wind Eng. Ind. Aerodyn.*, 49(1–3), 351–368.

Sonneville, P. (1973). "Étude du champ de pressions fluctuantes à la surface d'un cylindre circulaire." *C. R. Acad. des Sci. Paris, Sér. A*, 277, 383–385 (in French).

Szepessy, S., and Bearman, P. W. (1992). "Aspect ratio and end plate effects on vortex shedding from a circular cylinder." *J. Fluid Mech.*, 234, 191–217.

Vandoormaal, J. P., and Raithby, G. D. (1984). "Enhancements of the simple method for predicting incompressible fluid flows." *Numer. Heat Transfer*, 7(2), 147–163.

West, G. S., and Apelt, C. J. (1993). "Measurements of fluctuating pressures and forces on a circular cylinder in the Reynolds number range 10^4 to 2.5×10^5." *J. Fluids Struct.*, 7(3), 227–244.

Wieselsberger, C. (1921). "Neuere Feststellungen über die Gesetze des Flüssigkeits-und Luftwiderstands." *Physikalische Zeitschrift*, 22, 321–328 (in German).

Downloaded from ascelibrary.org by Iowa State University on 09/23/22. Copyright ASCE. For personal use only; all rights reserved.